SDC

DIRECTIONAL OPTICAL COHERENCE TOMOGRAPHY IMAGING OF MACULAR PATHOLOGY

BRANDON J. LUJAN, MD,* SHANE M. GRIFFIN, MD,† VIKRAM S. MAKHIJANI, DO,‡ BHAVNA J. ANTONY, PHD,§ EMILY Y. CHEW, MD,¶ AUSTIN ROORDA, PHD,** H. RICHARD MCDONALD, MD††

Purpose: To survey the impact of directional reflectivity on structures within optical coherence tomography images in retinal pathology.

Methods: Sets of commercial optical coherence tomography images taken from multiple pupil positions were analyzed. These directional optical coherence tomography sets revealed directionally reflective structures within the retina. After ensuring sufficient image quality, resulting hybrid and composite images were characterized by assessing the Henle fiber layer, outer nuclear layer, ellipsoid zone, and interdigitation zone. Additionally, hybrid images were reviewed for novel directionally reflective pathological features.

Results: Cross-sectional directional optical coherence tomography image sets were obtained in 75 eyes of 58 patients having a broad range of retinal pathologies. All cases showed improved visualization of the outer nuclear layer/Henle fiber layer interface, and outer nuclear layer thinning was, therefore, more apparent in several cases. The ellipsoid zone and interdigitation zone also demonstrated attenuation where a geometric impact of underlying pathology affected their orientation. Misdirected photoreceptors were also noted as a consistent direction-dependent change in ellipsoid zone reflectivity between regions of normal and absent ellipsoid zone.

Conclusion: Directional optical coherence tomography enhances the understanding of retinal anatomy and pathology. This optical contrast yields more accurate identification of retinal structures and possible imaging biomarkers for photoreceptor-related pathology.

RETINA 44:1124–1133, 2024

Optical coherence tomography (OCT) uses interferometry from reflected infrared light and has become the most frequently utilized diagnostic test in ophthalmology.[1] As OCT technology has advanced, images appear to match the level of detail present in histology. While it is tempting to consider retinal OCT images an "optical biopsy," the acquisition techniques performed can substantially alter their appearance and interpretation.

The optical property of directional reflectivity, where the illumination and reflection angles affect the appearance of tissue, initially focused on the ex vivo analysis of the retinal nerve fiber layer (NFL).[2] Subsequently, in vivo OCT imaging has demonstrated directional reflectivity in the NFL2, Henle fiber layer (HFL),[4,5] internal limiting membrane, and the photoreceptor outer retinal hyperreflective bands.[6]

First noted ex vivo by Anger et al,[7] the variable reflectivity of HFL may appear to be a limitation of OCT, however, its directional reflectivity can actually be leveraged to gain structural information. One approach to utilizing this, directional optical coherence tomography (D-OCT), can be performed by acquiring multiple OCT images through different pupil positions.[8] This technique was initially used in patients without macular pathology to obtain precise independent thickness measurements of the outer nuclear layer (ONL) and HFL.[9] Subsequently, D-OCT has been used in a few conditions to infer pathological alterations in photoreceptor orientation,[10–12] volumetric HFL mapping,[13] and NFL variability.[14] In this study, we acquired D-OCT images in patients over a much broader spectrum of retinal pathologies to investigate whether abnormal patterns of directional reflectivity may be observed.

Methods

Study Design

This was a retrospective observational case series.

Subjects

The study was approved by the Western Institutional Review Board, Puyallup, WA. We retrospectively reviewed imaging data from patients who were seen at West Coast Retina Medical Group with retinal diseases that affected the photoreceptor layers and who had undergone OCT imaging. Optical coherence tomography images obtained from an additional deidentified patient participating in an IRB-approved study from the National Eye Institute were included. All investigative procedures adhered to the tenets of the Declaration of Helsinki.

Directional Optical Coherence Tomography Imaging

Cross-sectional D-OCT sets were acquired using two commercially available Zeiss Cirrus HD-OCT (Dublin, CA) systems by multiple imagers using a technique previously shown to be highly reproducible.[15] Directional optical coherence tomography image sets consisted of a series of standard OCT images acquired through different pupil positions. For D-OCT sets, photographers imaged an HD-line scan through the pupil position that resulted in a "flat" horizontal OCT B-scan, which was also vertically centered in the pupil. Subsequently, the vertical position was maintained while acquiring horizontal images at decentered nasal and temporal pupillary positions at a distance sufficient to visualize directional changes but without decreasing signal strength.[4] A complementary procedure was implemented for vertically acquired scans using vertical displacements and maintaining central horizontal positions. Patients were repeatedly instructed to maintain fixation on the "center of the central fixation target" for each scan. As the purpose of the study was exploratory, a wide variety of retinal pathologies in patients capable of maintaining good fixation were imaged.

From the *Casey Eye Institute, Oregon Health & Science University, Portland, Oregon; †Department of Ophthalmology, California Pacific Medical Center, San Francisco, California; ‡Department of Ophthalmology, Southern California Permanente Medical Group, Los Angeles, California; §Federation University Australia, Mount Helen, VIC, Australia; ¶National Eye Institute, Bethesda, Maryland; **Herbert Wertheim School of Optometry and Vision Science, University of California, Berkeley, Berkeley, California; and ††West Coast Retina Medical Group, San Francisco, California.

None of the authors has any financial/conflicting interests to disclose.

Supplemental digital content is available for this article. Direct URL citations appear in the printed text and are provided in the HTML and PDF versions of this article on the journal's Web site (www.retinajournal.com).

Reprint requests: Brandon J. Lujan, MD, 545 SW Campus Drive, Portland, OR 97239; e-mail: brandonlujanmd@gmail.com

Directional Optical Coherence Tomography Analysis

Images with a signal strength of less than 8, with motion artifacts, or marked fixational instability were excluded. Included D-OCT sets were then registered and processed using custom software. Briefly, internal limiting membrane (ILM) segmentation was performed on each of the individual scans in the D-OCT set. Individual one-pixel width axial scans from the noncentral pupil locations were then shifted axially to match the position of the ILM segmentation contour from the central pupil location. The individual images within the registered image set were then intensity normalized using the reflectivity of the highly reflective and nondirectional inner plexiform layer as a reference to compensate for global reflectivity changes.

Directional Optical Coherence Tomography Visualization

Hybrid D-OCT images were created by giving each B-scan within the set a color channel while maintaining its pixel values. For horizontal images, temporally displaced, central, and nasally displaced scans of left eyes were converted to red, green, and blue (RGB), respectively. This RGB color assignment was maintained for the right eyes. An analogous analysis for vertically acquired images was employed with the inferior macula corresponding to temporally displaced left eyes. Images within the set were then combined to yield a hybrid D-OCT image, consisting of both colored and grayscale pixels. Composite D-OCT images were created from registered and normalized images by taking the maximum pixel value at each location from the three images and assigning that grayscale value to the resulting composite D-OCT image.

Results

A total of 98 D-OCT sets from 70 patients were imaged through multiple pupil entry positions. Of these, 23 sets were excluded due to poor signal strength, poor image registration, or another artifact; 75 D-OCT sets from 58 patients having various retinal pathologies were processed and analyzed further using registered B-scans, hybrid D-OCT images and composite D-OCT images. The entire set of data used in this analysis is presented in **Supplemental Digital Content 1** (see **Figure**, http://links.lww.com/IAE/C242).

Equal reflectivity from each pupil entry position—and therefore each color channel—meant a structure was nondirectionally reflective and resulted in predominantly grayscale pixels in hybrid D-OCT images.

However, if pixel values differed between the color channels, then those structures were determined to demonstrate directional reflectivity. Consequently, directionally reflective and nondirectionally reflective structures could be visualized in a single image.

Directionally reflective structures included HFL, inner-segment/outer-segment junction or ellipsoid zone (EZ), outer-segment tips or interdigitation zone (IZ), NFL, and in some cases, pathological material (Figures 1–5). All hybrid D-OCT images demonstrated an improved visualization of the HFL/ONL interface. Ellipsoid zone and IZ reflectivities were found to be altered by pathological features in addition to the expected directional reflectivity of off-axis acquisition.[6] We qualitatively assessed the impact of these features across 32 different pathologies, as listed in Table 1. We determined whether the composite D-OCT image had a significant (++), mild (+), or no effect (0) on the visibility of the EZ and IZ compared with using a single flat OCT image. Several key cases epitomize some consistent findings observed over the breadth of the pathologies analyzed.

Case 1: Best Vitelliform Dystrophy

Figure 1 is a patient with best vitelliform dystrophy. On standard OCT imaging, there is subretinal fluid (SRF), a partially atrophic retinal pigment epithelium (RPE), and increased choroidal hypertransmission. Ellipsoid zone hyperreflectivity was limited to the central fovea overlying the SRF. However, displacing the OCT beam through the pupil nasally and temporally revealed additional EZ reflectivity along the sides of the vitelliform lesion. Hybrid D-OCT images demonstrated a continuous EZ consisting of different orientations and directionally reflective subretinal material. A composite D-OCT image demonstrates a continuous EZ, in sharp distinction to the standard OCT image.

Case 2: Nonexudative Age-Related Macular Degeneration

A patient with age-related macular degeneration (AMD) and complete retinal pigment epithelial and outer retinal atrophy or geographic atrophy (GA) is shown in Figure 2. Surrounding the areas of

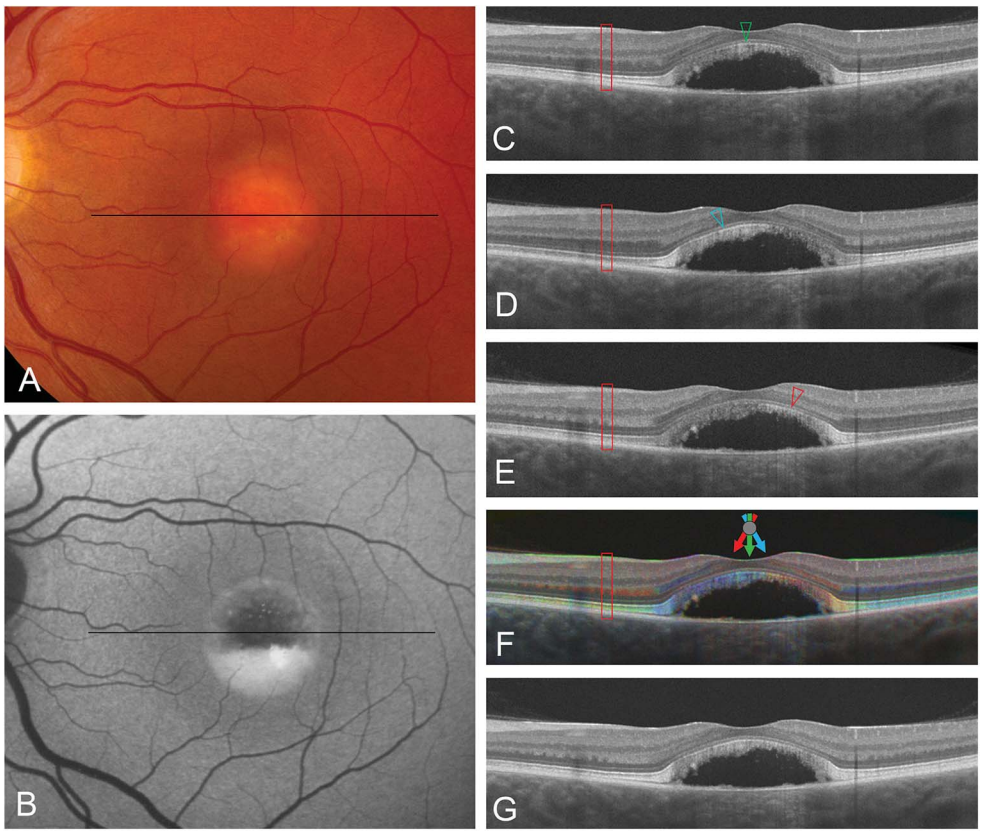

Fig. 1. Best vitelliform dystrophy. **A.** Color fundus photograph of left eye demonstrating central macular vitelliform lesion. **B.** Blue-light fundus autofluorescence image showing hyperautofluorescent material circumscribing lesion superior and lateral edges and settling inferiorly. **C.** Standard horizontal OCT image through the center of the pupil demonstrating SRF and best lesion at the location of lines in (**A** and **B**). The green arrowhead indicates the central direction of light incident on the retina and the central hyperreflective EZ. The red rectangle indicates standard retinal OCT layers. **D.** OCT image acquired through nasal pupil aligned to the image in (**C**). The blue arrowhead indicates the direction of light incident on the retina and the hyperreflective EZ on the nasal aspect of the best lesion. The red rectangle indicates hyporeflective HFL, decreased reflectivity of EZ, and almost absent reflectivity from IZ compared with (**C**). **E.** OCT image acquired through temporal pupil aligned to the image in (**C**). The red arrowhead indicates the direction of light incident on the retina and the hyperreflectivity of EZ on the temporal aspect of the best lesion. The red rectangle shows hyperreflective HFL, decreased EZ, and markedly reduced IZ compared with (**C**). **F.** D-OCT hybrid image comparing reflectivity by position from (**C**–**E**). Variable reflectivity of EZ by orientation is demonstrated overlying vitelliform lesion. Structures within the red rectangle that demonstrate strong directional reflectance include internal limiting membrane, HFL, EZ, and IZ. **G.** Composite image demonstrating maximum reflectivity from (**C**–**E**) demonstrating relatively intact EZ and thinned ONL below HFL.

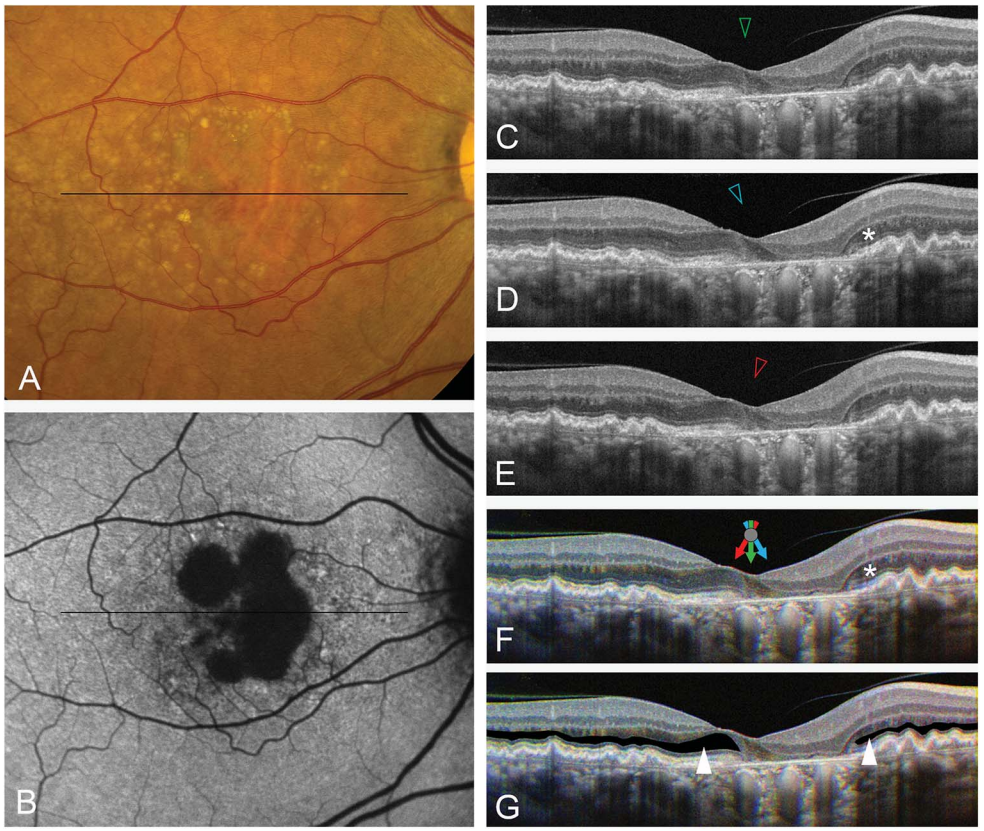

Fig. 2. Nonexudative AMD with GA. **A.** Color fundus photograph of right eye demonstrating drusen and central GA. **B.** Blue-light fundus autofluorescence image showing drusen and a multifocal area of hypoautofluorescent GA. **C.** Standard horizontal OCT image through the center of the pupil as indicated by a green arrowhead at location of lines in (**A** and **B**) showing drusen and RPE loss and choroidal hypertransmission. **D.** Blue arrowhead indicating OCT image acquired through temporal pupil aligned to the image in (**C**). Hyperreflective nasal HFL and an increase in EZ reflectivity on the nasal slope of drusen adjacent GA (asterisk) are visible. **E.** Red arrowhead demonstrating nasal entry OCT image aligned to the image in (**C**) showing hyperreflective temporal HFL compared with (**C**). **F.** D-OCT hybrid image comparing the reflectivity of (**C**–**E**). Photoreceptor orientation irregularity demonstrated by color variation across EZ, particularly adjacent atrophy (asterisk). **G.** Improved visualization of ONL/HFL interface allows precise demarcation of ONL (in black) not apparent in (**C**).

photoreceptor loss are hyporeflective structures on standard OCT that can be seen to comprise directionally reflective HFL by their rainbow appearance of cascading reflectivity on D-OCT. The underlying hyporeflective tissue was precisely identified as ONL. In addition, changes in the color of the EZ overlying drusen and at the edges of the GA suggest photoreceptor misdirection away from the pupillary center.

Case 3: Macular Telangiectasia Type 2

A patient with macular telangiectasia type 2 (MacTel) was imaged using D-OCT in Figure 3. Standard OCT imaging demonstrated features classic of MacTel including an inner lamellar cyst and temporal loss of photoreceptor outer retinal hyperreflective bands. In the nasal and temporal zones immediately adjacent to this area of frank loss, there was a marked change in reflectivity of the EZ and IZ depending on the angle of orientation. Specifically, reflectivity in the flanking zones was seen to decrease on nasal light entry and increase on temporal light entry relative to the standard central entry position. These regions of consistent alterations in reflectivity imply a uniform temporal misdirection of photoreceptors around the established area of definite EZ loss.

Case 4: Central Serous Chorioretinopathy

A patient with incomplete recovery from acute central serous chorioretinopathy is shown in Figure 4. While SRF had resolved after 6 weeks, there was a significant alteration in the photoreceptor orientation visible. Analysis of similar D-OCT images in conjunction with adaptive optics imaging of this eye was previously reported, and it demonstrated abnormalities in these areas using a split-detection system.[10] Previously unreported in this eye was the extent of subfoveal and perifoveal ONL loss and the comparison to the fellow eye.

Additional eyes with retinal pathology were imaged to assess the utility of this technique, look for general principles regarding the application of using directional reflectivity, and provide insight into underlying anatomical and pathophysiological changes. Table 1 lists the conditions assessed and Figure 5 provides additional examples of retinal pathology.

Discussion

Directional reflectivity is a fundamental optical property that must be considered to correctly assess

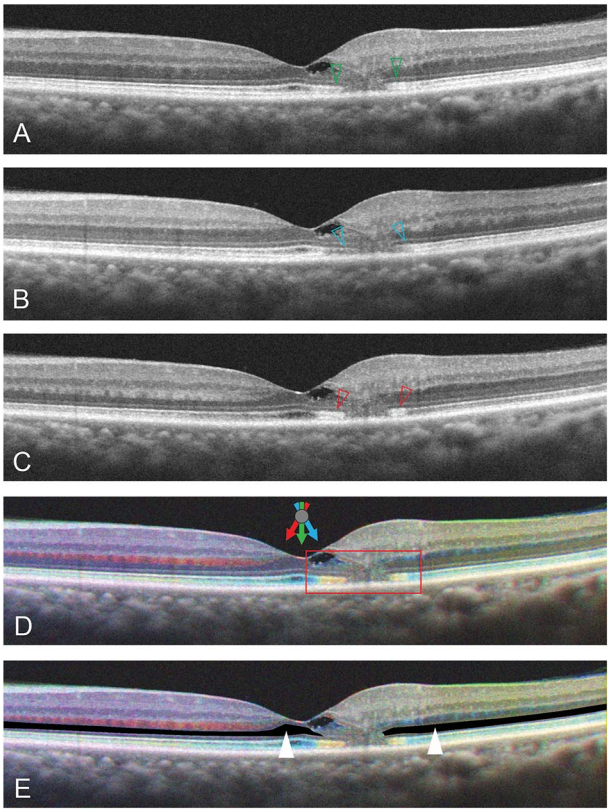

Fig. 3. MacTel. **A.** Standard horizontal OCT image demonstrates classic MacTel features of inner lamellar cystic space and discrete outer retinal loss. Sharply demarcated EZ edge indicated with the direction of entering light by green arrowheads. **B.** OCT image with nasal light entry demonstrating temporal HFL hyperreflectivity and a marked decrease in reflectivity of EZ and IZ at the cusps of frank EZ loss indicated by blue arrows. **C.** OCT image with temporal light entry demonstrating temporal HFL hyporeflectivity and a marked increase in reflectivity of EZ and IZ at cusps of frank EZ loss. **D.** Hybrid D-OCT image demonstrating predominantly green EZ except at cusps of the area of frank EZ loss where maximal reflectivity from temporal direction causes a red coloration, indicating photoreceptor misdirection. **E.** Hybrid D-OCT image demonstrates improved visualization of ONL/HFL, but no appreciable change in the EZ compared with standard horizontal entry.

OCT images. Fortunately, these attributes can be harnessed to reveal critical anatomical and orientation features of macular pathology which remain concealed by standard OCT imaging. We have presented a spectrum of retinal conditions where the utilization of directional reflectivity by D-OCT provided a clearer assessment of images and additional disease insights. For retina specialists, the impact of directional reflectivity on OCT layers associated with photoreceptors—the ONL, HFL, synaptic outer plexiform layer, EZ, and IZ—is paramount.

Without photoreceptors, there is no vision. Photoreceptor nuclei comprising the ONL are required for photoreceptor cell function, and ONL thickness measurements are the gold standard for histologically assessing photoreceptor degenerations. HFL, on the other hand, contains the axons of these photoreceptor nuclei as well as the Müller cells that support them. The synaptic outer plexiform layer contains only synapses and the deep vascular plexus. These three structures are very different anatomically, functionally, and optically and should not be grouped together. Previous studies of normal patients have demonstrated that the cross-sectional thickness[9] and volumes[13] of these layers do not correlate by eccentricity in a given patient or between patients. Outer nuclear layer thinning does not mirror the Müller cell containing HFL loss in GA in cases where these structures can be histologically separated.[16] Furthermore, pathological studies of diseased eyes have demonstrated that these layers may thicken and thin independently, presumably because of the persistence of Müller cell processes in HFL.[16,17] Consequently, grouping them together as ONL + HFL or ONL+ results in a loss of potentially critical information.

The dry AMD eye in Case 2 demonstrates the use of D-OCT to clearly disambiguate ONL from HFL, which allowed the precise layer thickness of degenerating nuclei to be assessed, critical to a complete understanding of AMD pathogenesis. Bird et al[18] demonstrated that ONL loss occurs not just within and at the RPE atrophy border in eyes with GA, but also away from the region of RPE atrophy. Once size thresholds are met, the consensus terms of complete and incomplete retinal pigment epithelial and outer retinal atrophy (cRORA and iRORA, respectively[19]) contain an immense range of phenotypes within each classification. Accurate quantitative assessments of ONL thicknesses throughout the macula would likely provide significant additional diagnostic and prognostic advantages. Clinical studies of retinal degenerations and AMD have demonstrated thinned ONL; however, true ONL loss may be drastically underrepresented because residual HFL and ONL are measured together. Dyslamination, the loss of distinction between these layers which has been observed histopathologically,[16] may confound precise measures, but it may also offer a unique optical signature on D-OCT imaging and should be a topic of future investigation.

Algorithms that can predict the development of atrophy have unnecessarily handicapped themselves by grouping these layers and may improve their predictive potential by optically isolating ONL. Existing segmentation algorithms variably include HFL based on how distinct its boundary is with adjacent ONL or outer plexiform layer, decreasing precision and confounding results.[20] Precisely identifying this boundary may someday be accomplished retrospectively by artificial intelligence[21] or research-grade systems with optical innovations,[22] but this can already be

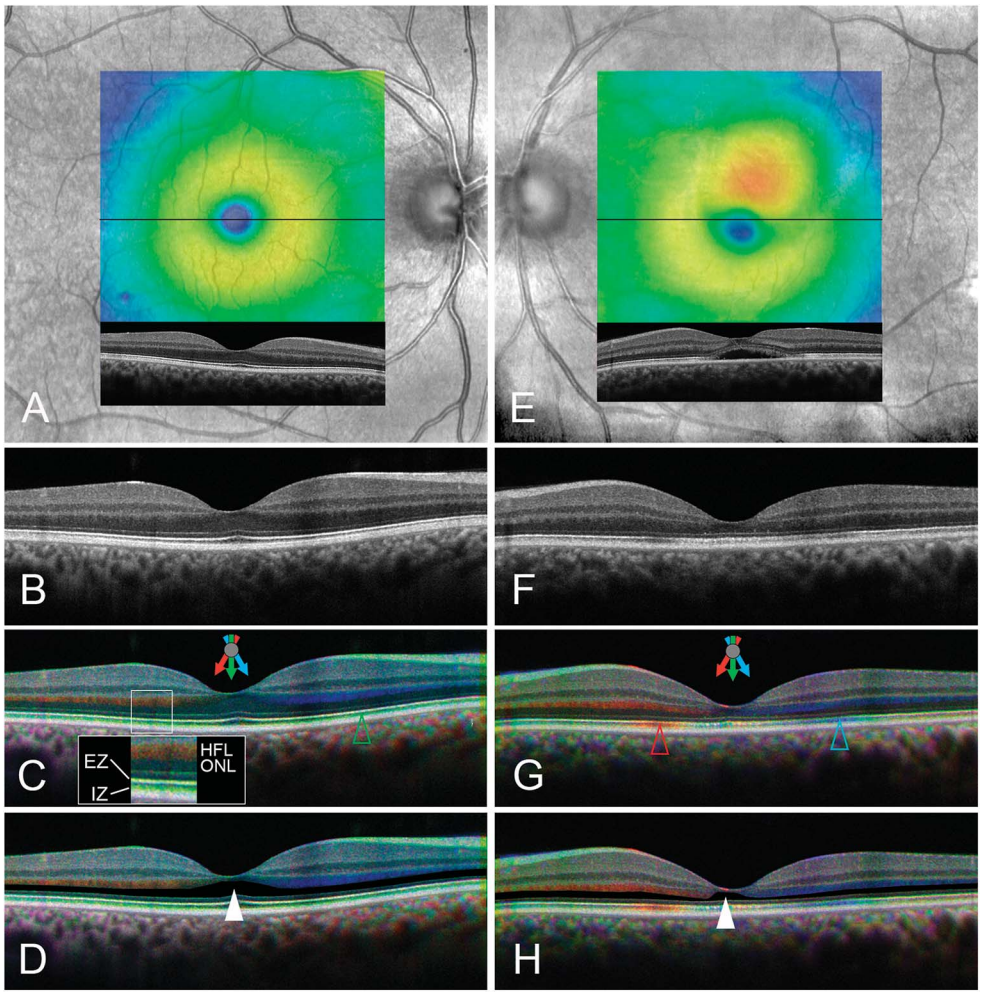

Fig. 4. Resolved central serious chorioretinopathy. **A.** Normal fellow eye of patient with recovered central serious chorioretinopathy showing macular thickness map and central horizontal OCT in **B**. **C.** Hybrid D-OCT image showing normal HFL and EZ directional reflectivity (green arrowheads). Inset demonstrates structures normally impacted by directional reflectivity: EZ, IZ, HFL, and ONL. **D.** Hybrid D-OCT image allows clear delineation of ONL in black (white arrowhead). **E.** Appearance of acute central serious chorioretinopathy with subfoveal SRF. **F.** After the resolution of SRF 6 weeks later, central ONL thinning is apparent, with some apparent attenuation of EZ at the lateral extent of resolved SRF. **G.** Hybrid D-OCT reveals present but misaligned photoreceptors (red and blue arrowheads). **H.** Extent of ONL thinning (white arrowhead) is more apparent using hybrid D-OCT image.

accomplished using commercially available systems just by modifying acquisition parameters.

Unambiguous visualization of HFL can occur in several situations. In scans that are acquired off-axis, HFL becomes hyperreflective and hyporeflective on the contralateral and ipsilateral sides, respectively. In addition, this study demonstrates that loss of underlying ONL, pigment epithelial detachments, drusen, fluid, or focal choroidal excavation all produce similar changes in reflectivity even in the central scan, as the relative angle of incidence of the HFL fibers to the scanning beam becomes altered. Finally, ischemia of HFL can cause its hyperreflective appearance independently of the angle of incidence.[23] Use of D-OCT can disambiguate ischemia from hyperreflectivity caused by scanning angle or anatomical alteration to avoid misinterpretation by purposefully adding optical contrast (acute macular neuroretinopathy, Figure 5F).

The outer retinal hyperreflective bands are tempting imaging biomarkers for the diagnosis and progression of multiple retinal diseases. However, photoreceptor inner and outer segments have unique optical properties that require a nuanced approach toward their interpretation in OCT images.[24] The optical Stiles–Crawford effect is a consequence of photoreceptors acting as waveguides, and the EZ and IZ are maximally reflective when light is oriented directly on the axis to the photoreceptors.[6] Off-axis scans will therefore diminish the reflectivity of the EZ and IZ independent of any retinal pathology.[6,9,25] Lack of standardization of acquisition angle and its impact on reflectivity from these bands has been identified as a potential limitation of this biomarker.[26] At a minimum, given the directional reflectivity effects, OCT scan position should be controlled in clinical trials.

A decrease in EZ and IZ reflectivity at the central acquisition position compared with off-axis positions indicates photoreceptor misdirection. Eyes with the diagnosis of GA, MacTel, cone dystrophy, and retinitis pigmentosa demonstrate photoreceptor misdirection at

Table 1. Macular Pathologies Imaged

Pathology	Supplement Number(s)	ONL, HFL Findings	EZ, IZ Findings	EZ, IZ Changed in Composite?	Additional Findings
AMD, exudative: active	1, 2, 3	Diffuse ONL thinning	Misdirected EZ overlying fibrovascular PED and SRF	++	DiR "shaggy" photoreceptor material in subretinal space, non-DiR fibrosis
AMD, exudative: fibrosis	4	Diffuse ONL thinning	EZ misdirection adjacent atrophy and fibrosis	0	Non-DiR fibrosis
AMD, nonexudative: drusen	5, 6, 7, 8, 9, 10, 11	Focal ONL thinning, over drusen, geometric HFL	Misdirected EZ on drusen shoulders	+	DiR subretinal material
AMD, nonexudative: GA	12, 13, 14	Marked ONL thinning, HFL rainbows adjacent atrophy	EZ misdirection adjacent atrophy and overlying drusen	0	Figure 2
AMD, PED, and vitelliform	15	Focal ONL thinning	Misdirected and recoverable EZ, distinguishable from vitelliform	+	Non-DiR pseudovitelliform material
AMN, acute and resolved	16, 17	Abnormal HFL visibility acutely	Focal EZ misdirection and disruption	+	Figure 5F
AOFPED	18, 19	Focal ONL thinning centrally	EZ misdirection adjacent pigment	+	Non-DiR subfoveolar pigment
AOVMD	20, 21, 22, 23	Focal ONL thinning centrally	EZ, IZ misdirection	++	DiR and non-DiR subretinal material
APMPPE, chronic	24	Thin ONL overlying involved lesions, intact HFL	Central EZ, IZ misdirection	+	Non-DiR fibrotic change in RPE
Best vitelliform	25, 26, 27, 28	Thin central ONL	Misdirected EZ, IZ thickening	++	Figure 1
Commotio retinae	29	Central non-DiR HFL hyperreflectivity, ONL hyperreflectivity overlying SRF	Non-DiR EZ at boundary SRF	+	
Cone dystrophy	30, 31	Zones of complete ONL and HFL loss, HFL rainbows at edges	Misdirected EZ at edges, centrally	+	Figure 5D
Contralateral eye of unilateral RP	32	Unremarkable	Central EZ, IZ misdirection	0	Increased EZ, IZ reflectivity
CSCR-acute	33, 34, 35, 26, 37	Geometric HFL	Misdirected recoverable EZ	++	Figure 5C
CSCR-chronic	38, 39, 40, 41	Marked ONL thinning	Persistent EZ, IZ misdirection and loss	+	Figure 4
Epiretinal membrane	42	Unremarkable	Parafoveal EZ, IZ misdirection	0	DiR cotton ball sign
FCE/CSCR	43	Expanded and geometric HFL	EZ misdirection	+	
Ganglioma/ astrocytoma	44	Thinned HFL	Unremarkable	0	DiR material in GCL and NFL
Lamellar hole	45	Ragged central ONL	Central EZ, IZ misdirection	++	OPL schisis visible on volume images
Macular telangiectasia type 2	46, 47, 48, 49, 50, 51, 52	Focal ONL thinning, increased and abnormal HFL, and sOPL visibility	Increased perilesional decrease in reflectivity, EZ, IZ misdirection	+	Figure 3
MEWDS, acute and resolving	53, 54, 55	Focal non-DiR HFL hyperreflectivity acutely	EZ misdirection while resolving	+	Acute non-DiR lumps/ bumps in outer retina
Optic atrophy with INL pseudocysts	56	Unremarkable	Unremarkable	0	Non-DiR INL cysts, thickened synaptic OPL
PAMM secondary to BRAO	57, 58	DiR HFL underlying PAMM	Unremarkable acutely, misdirected during resolution	0	Non-DiR PAMM acutely, becomes DiR during resolution
PAMM secondary to CRVO, incidental CNV	59	Geometric HFL	EZ misdirection overlying fibrovascular PED	+	DiR HFL underlying PAMM
PAMM, resolved	60, 61	Non-DiR HFL enlargement into prior ischemic area	EZ, IZ misdirection	0	Foveal non-DiR NFL/ GCL/IPL/INL thinning
Pattern dystrophy	62	ONL thinning, HFL rainbow at edges	EZ misdirection adjacent lesion	0	Figure 5B
Plaquenil toxicity	63, 64	Severe ONL thinning	EZ, IZ misdirection centrally, perifoveal EZ, IZ loss	+	

Table 1. (*Continued*)

Pathology	Supplement Number(s)	ONL, HFL Findings	EZ, IZ Findings	EZ, IZ Changed in Composite?	Additional Findings
Retinitis pigmentosa	65, 66, 67, 68, 69	Diffuse ONL thinning increasing with eccentricity	Diffuse EZ misalignment, and eccentric loss	0	
Retinal detachment repair	70, 71	Diffuse ONL thinning	EZ, IZ misdirection	++	Figure 5E
Unknown1	72	Granular DiR material in ONL	Central EZ misdirection	0	Prominent middle limiting membrane
Unknown2	73	Central ONL thinning	Misdirection at edges of EZ loss	+	DiR material above foveal cavitation
Unknown3	74	Unremarkable thickness	Focal EZ hyperreflectivity and misdirection	0	Fine granular material in central ONL
VKH with BALAD	75	Diffuse ONL thinning	EZ misdirection overlying SRF	+	Non-DiR BALAD, DiR material overlying RPE under BALAD

AMN, acute macular neuroretinopathy; AOFPED, adult-onset foveolar pigment epithelial dystrophy; AOVMD, adult-onset vitelliform macular dystrophy; APMPPE, acute posterior multifocal placoid pigment epitheliopathy; BALAD, bacillary layer detachment; BRAO, branch retinal artery occlusion; CNV, choroidal neovascularization; CRVO, central retinal vein occlusion; DiR, directionally reflective; ELM, external limiting membrane; EZ, ellipsoid zone (inner-segment/outer-segment junction); FCE, focal choroidal excavation; GCL, ganglion cell layer; INL, inner nuclear layer; IPL, inner plexiform layer; IZ, interdigitation zone (outer-segment tips); MEWDS, multiple evanescent white dot syndrome; OPL, outer plexiform layer; PAMM, paracentral acute middle maculopathy; PED, pigment epithelial detachment; RP, retinitis pigmentosa; VKH, Vogt-Koyanagi-Harada disease.

the boundary between normal appearing EZ and where there is definite EZ loss. These regions may represent "distressed" photoreceptors, and clinical trials should utilize D-OCT to gather additional insight into the progression of photoreceptor loss in these zones. Misdirected photoreceptors may represent a novel imaging biomarker and define regions of photoreceptor cells that still have the potential to be rescued by future therapies. "EZ At-risk" has been proposed as a biomarker for the progression of EZ loss in AMD[27] and other conditions. It is possible that this represents photoreceptor misdirection and should be correlated to the EZ changes visualized in dry AMD and in MacTel in Figure 3.

Drusen may also have a component of photoreceptor misdirection as well, as shown in Figure 5A. However, early studies of D-OCT of drusen have also shown that EZ is truly diminished overlying them after accounting for directional effects[28] and is also reduced in regions of EZ between drusen in AMD eyes.[29] Future larger investigations should be undertaken to assess photoreceptor reflectivity in dry AMD.

In eyes with retinal pathology and altered RPE geometry where some preservation of true ONL exists, a decrease in EZ signal on standard OCT imaging cannot conclusively be interpreted as photoreceptor loss. As seen in Figure 1, the EZ signal may be recoverable when imaged off-axis. Presumably, the inner and outer segments were oriented away from the central pupil and only reflected light to the detector when eccentric pupil positions aligning with the photoreceptor axes were used. The use of a composite image taken from multiple pupil positions, therefore, provides a more comprehensive assessment of the EZ than would be available from a single OCT image.

The utilization of knowledge of directional reflectivity and waveguiding properties allows for an enhanced assessment of ambiguous structures. Advances in regenerative cell and gene therapy for the retina have led to the identification of emergent hyperreflective structures. However, the components of these bands above the RPE are speculative. The detection of an EZ or IZ optical signature of directional reflectivity could be the imaging biomarker for concluding that these bands are due to photoreceptors. While its use in retinal regeneration is only beginning, there are immediate applications of D-OCT for the interpretation of ambiguous structures. For example, in best vitelliform dystrophy (Figure 1) and in acute central serous chorioretinopathy (Figure 5B), the subretinal material follows the pattern of reflectivity found in the EZ and IZ, indicating it may include photoreceptor components.

Limitations of this study include the small number of patients included with each diagnosis, the use of commercial hardware, and analysis methods. While the attempt of this study was to survey retinal pathology with D-OCT, patients imaged with a given diagnosis are not necessarily representative of each condition. Indeed, the requirement for excellent fixation excluded patients with advanced disease affecting

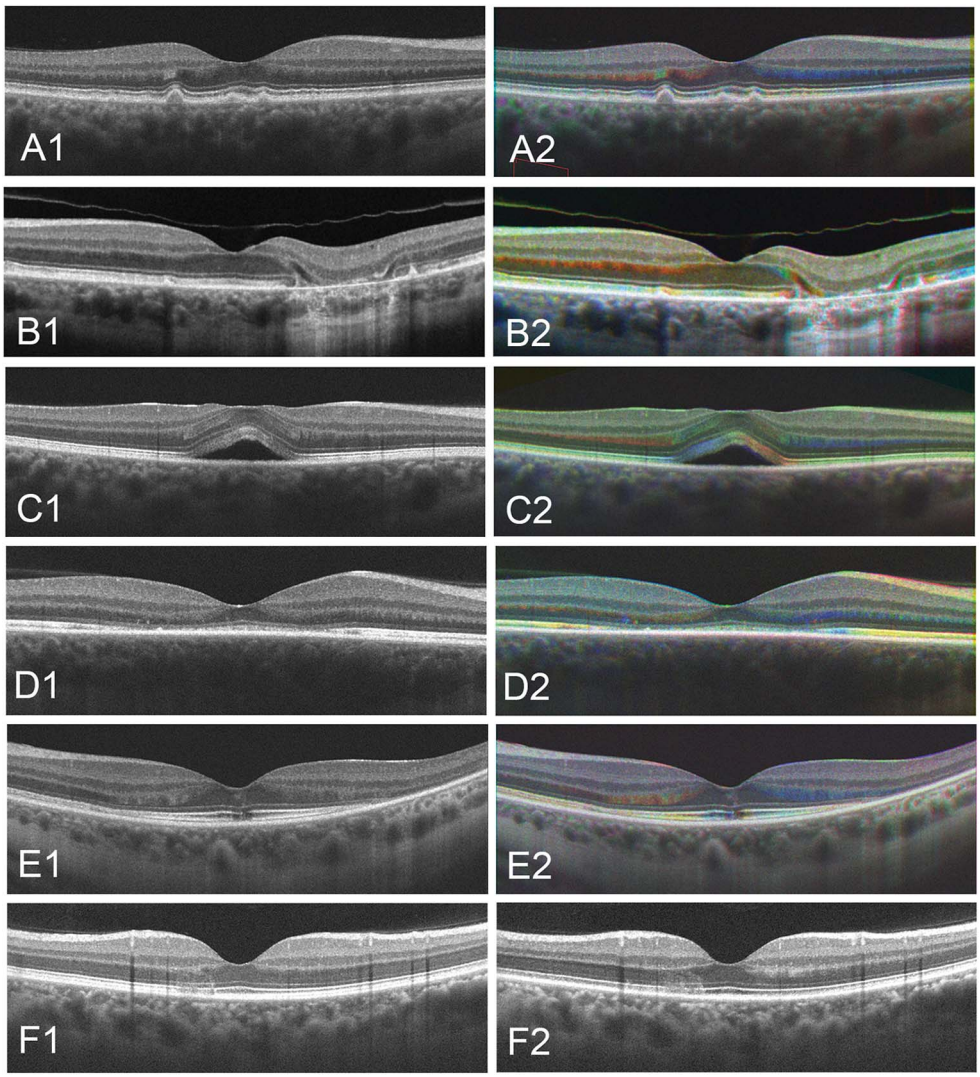

Fig. 5. Spectrum of standard OCT compared with hybrid D-OCT images. **A1**. Non-exudative AMD. **A2**. Altered alignment of EZ apparent as well as thinned ONL and variably thickened and thinned HFL. **B1**. Pattern dystrophy with RPE atrophy. **B2**. Clear edge of ONL loss temporally visible with rainbow HFL appearance on either side of atrophy. Misdirected EZ apparent at the edge of atrophy. **C1**. Acute central serous chorioretinopathy. **C2**. Expected geometric alterations of HFL and EZ due to the presence of SRF. Shaggy subretinal material also demonstrates photoreceptor EZ D-OCT signature. **D1**. Cone dystrophy. **D2**. Central EZ loss and misdirection at its edges. True extent of ONL loss apparent as well as expected geometric variation in the appearance of HFL. **E1**. Retinal detachment repair. **E2**. Extent of ONL loss apparent. Central IZ misdirection surrounding frank EZ and IZ loss centrally. **F1**. Acute macular neuroretinopathy, standard vertical OCT demonstrating disruption of EZ and hyperreflective HFL, ONL, and external limiting membrane. **F2**. Registered off-axis D-OCT through inferior pupil demonstrating more clearly the extent of HFL hyperreflectivity in the context of expected hyporeflective inferior HFL.

foveal photoreceptors. Subtle fixational changes of the patient while manually moving the commercial OCT device between pupil positions limited the value of imperfectly registered D-OCT sets. This current limitation of commercial OCT systems would clearly be aided by the incorporation of robust eye-tracking, increased scan speed capable of volumetric imaging,[30] or by research-grade systems having multiple beams.[14] Dedicated hardware capable of rapidly steering the OCT beam through numerous pupil entry positions would have the additional advantage of allowing composite D-OCT images to create EZ reflectivity profiles, instead of what is practical using current commercial systems.

Further improvements in hybrid and composite image analysis would aid in quantitative analysis in individuals and within cohorts. Currently, these were not standardized by pupil entry position relative to the optical axis of a given eye, and the angles used were necessarily individualized to patients by balancing image "tilt" and loss of signal strength. Because this imaging angle could differ between nasal and temporal directions, the chromatic hybridization may be biased toward more off-axis scan positions. Despite this, changes in directional reflectivity could clearly be detected and rough photoreceptor orientation determined.

All future clinical trials addressing the anatomical status of photoreceptors would benefit from using D-OCT to assess the true ONL thickness and fully assess the outer retinal hyperreflective bands. This imaging technique may more precisely measure change and has the potential to predict future loss of photoreceptors as a biomarker for progression. Advances in hardware and software solutions may provide deeper clinical insights into the specific macular

pathologies that this study surveys and drive the utilization of directional reflectivity as an improvement on standard OCT imaging.

Key words: reflectivity, retina, photoreceptor, Henle fiber layer, outer nuclear layer, ellipsoid zone, age-related macular degeneration, geographic atrophy, best disease, macular telangiectasia.

Acknowledgments

The authors gratefully acknowledge the contributions of Robert W. Knighton, PhD in reviewing this work. Supported by Grant P30 EY010572 from the National Institutes of Health (Bethesda, MD) and by unrestricted departmental funding from Research to Prevent Blindness (New York, NY).

References

1. Huang D, Swanson EA, Lin CP, et al. Optical coherence tomography. Science 1991;254:1178–1181.
2. Knighton RW, Baverez C, Bhattacharya A. The directional reflectance of the retinal nerve fiber layer of the toad. Invest Ophthalmol Vis Sci 1992;33:2603–2611.
3. Knighton RW, Qian C. An optical model of the human retinal nerve fiber layer: implications of directional reflectance for variability of clinical measurements. J Glaucoma 2000;9:56–62.
4. Lujan BJ, Roorda A, Knighton RW, Carroll J. Revealing Henle's fiber layer using spectral domain optical coherence tomography. Invest Ophthalmol Vis Sci 2011;52:1486–1492.
5. Otani T, Yamaguchi Y, Kishi S. Improved visualization of Henle fiber layer by changing the measurement beam angle on optical coherence tomography. Retina 2011;31:497–501.
6. Gao W, Cense B, Zhang Y, et al. Measuring retinal contributions to the optical Stiles-Crawford effect with optical coherence tomography. Opt Express 2008;16:6486–6501.
7. Anger EM, Unterhuber A, Hermann B, et al. Ultrahigh resolution optical coherence tomography of the monkey fovea. Identification of retinal sublayers by correlation with semithin histology sections. Exp Eye Res 2004;78:1117–1125.
8. Makhijani VS, Roorda A, Bayabo JK, et al. Chromatic visualization of reflectivity variance within hybridized directional OCT images. In: *Proceedings of Society of Photo-Optical Instrumentation Engineers, p. 8571; Optical Coherence Tomography and Coherence Domain Optical Methods in Biomedicine XVII, p. 857105; March 20, 2013*.
9. Lujan BJ, Roorda A, Croskrey JA, et al. Directional optical coherence tomography provides accurate outer nuclear layer and Henle fiber layer measurements. Retina 2015;35:1511–1520.
10. Sun LW, Carroll J, Lujan BJ. Photoreceptor disruption and vision loss associated with central serous retinopathy. Am J Ophthalmol Case Rep 2017;8:74–77.
11. Rossant F, Grieve K, Paques M. Highlighting directional reflectance properties of retinal substructures from D-OCT images. IEEE Trans Biomed Eng 2019;66:3105–3118.
12. Paques M, Rossant F, Finocchio L, et al. Attenuation outer retinal bands on optical coherence tomography following macular edema: a possible manifestation of photoreceptor misalignment. Retina 2020;40:2232–2239.
13. Kesim C, Bektas SN, Kulali Z, et al. Henle fiber layer mapping with directional optical coherence tomography. Retina 2022; 42:1780–1787.
14. Wartak A, Augustin M, Haindl R, et al. Multi-directional optical coherence tomography for retinal imaging. Biomed Opt Express 2017;8:5560–5578.
15. Tong KK, Lujan BJ, Zhou Y, Lin MC. Directional optical coherence tomography reveals reliable outer nuclear layer measurements. Optom Vis Sci 2016;93:714–719.
16. Li M, Huisingh C, Messinger J, et al. Histology of geographic atrophy secondary to age-related macular degeneration a multilayer approach. Retina 2018;38:1937–1953.
17. Sadigh S, Cideciyan AV, Sumaroka A, et al. Abnormal thickening as well as thinning of the photoreceptor layer in intermediate age-related macular degeneration. Invest Ophthalmol Vis Sci 2013;54:1603–1612.
18. Bird AC, Phillips RL, Hageman GS. Geographic atrophy: a histopathological assessment. JAMA Ophthalmol 2014;132:338–345.
19. Sadda SR, Guymer R, Holz FG, et al. Consensus definition for atrophy associated with age-related macular degeneration on OCT: classification of atrophy report 3. Ophthalmology 2018; 125:537–548.
20. Garvin MK, Abramoff MD, Wu X, et al. Automated 3-D intraretinal layer segmentation of macular spectral-domain optical coherence tomography images. IEEE Trans Med Imaging 2009;28:1436–1447.
21. Cansiz S, Kesim C, Bektas SN, et al. *FourierNet:* shape-preserving network for Henle's fiber layer segmentation in optical coherence tomography images. IEEE J Biomed Health Inform 2023;27:1036–1047.
22. Valente D, Vienola KV, Zawadzki RJ, Jonnal RS. Simultaneous directional full-field OCT using path-length and carrier multiplexing. Opt Express 2021;29:32179–32195.
23. Ramtohul P, Cabral D, Sadda S, et al. The OCT angular sign of Henle fiber layer (HFL) hyperreflectivity (ASHH) and the pathoanatomy of the HFL in macular disease. Prog Retin Eye Res 2023;95:101135.
24. Jonnal RS, Kocaoglu OP, Zawadzki RJ, et al. The cellular origins of the outer retinal bands in optical coherence tomography images. Invest Ophthalmol Vis Sci 2014;55: 7904–7918.
25. Park D, Lujan BJ. Normal interdigitation zone loss by motion-tracked OCT. Ophthalmol Retina 2017;1:394.
26. Lee KE, Heitkotter H, Carroll J. Challenges associated with ellipsoid zone intensity measurements using optical coherence tomography. Transl Vis Sci Technol 2021;10:27.
27. Kalra G, Cetin H, Whitney J, et al. Automated identification and segmentation of ellipsoid zone at-risk using deep learning on SD-OCT for predicting progression in dry AMD. Diagnostics (Basel) 2023;13:1178.
28. Marsh-Armstrong B, Murrell KS, Valente D, Jonnal RS. Using directional OCT to analyze photoreceptor visibility over AMD-related drusen. Sci Rep 2022;12:9763.
29. Griffin SM, Jia Y, Johnson AJ, et al. Directional reflectivity of the ellipsoid zone in dry age-related macular degeneration. Ophthalmic Surg Lasers Imaging Retina 2021;52:145–152.
30. Ni S, Khan S, Nguyen TTP, et al. Volumetric directional optical coherence tomography. Biomed Opt Express 2022;13:950–961.